To test these predictions we used drops of distilled water which contained charge-stabilized surfactant-free polystyrene microspheres (Interfacial Dynamics, Portland, OR) at a starting volume fraction of 10^{-4}. The spheres were so dilute that they could be regarded as an ideal solution except in the very narrow region occupied by the ring. Droplets with nominal radius 2 mm were deposited on glass microscope slides and allowed to dry in a large enclosure with measured ambient temperature and humidity. The volume of the droplet was inferred by weighing the slide during drying. The volume decreased at a rate which agreed within 2% with that expected for steady-state vapour-diffusion-limited evaporation, using tabulated values[10] for the water diffusivity in air and for the saturated vapour concentration.

In a separate experiment we observed the solute ring deposition by viewing the migration of 1-μm microspheres in a video microscope during drying (Fig. 1b). By automatically analysing[11] the video record, the depth-averaged velocity $\bar{v}(r)$ and the number of particles in the ring $M(R, t)$ were measured. Contact-line pinning is produced by surface irregularities and is much stronger with the solute than without it. The ring deposit can create surface unevenness as well as augment the surface imperfections that produced the initial pinning.

The depth-averaged velocity $\bar{v}(r)$ for thin drops, with $\theta_c \approx 0$, shows the predicted $(R - r)^{-0.5}$ divergence in the vicinity of the contact line. The measured ring mass $M(R, t)$ is plotted in Fig. 3. These drops had an initial contact angle $\theta_c \approx 0.25$ radians. For this angle, our theory predicts an initial increase $M(R, t) \approx t^{1.37}$. This behaviour is not expected at very early times ($t \lesssim (4R)^2/D \approx 10$ s), before steady-state diffusion has been achieved. To account for transient effects during this early period, we allow a shift in the effective starting time of the order of 10 s. We also include an offset in the deposited mass to account for the particles deposited during the initial transient. Choosing the M and t offsets to achieve the best straight line on a log–log plot yielded power-law fits $M - M_0 \approx (t + t_0)^p$, where $p = 1.3 \pm 0.1$. Thus the expected initial growth of the ring is consistent with observation. To predict the growth of the ring at later times, we first determine $\bar{v}(r)$ numerically from the known flux $J(r)$ of a thick drop and then use this $\bar{v}(r)$ to determine $M(R, t)$ as outlined in equation (1) above. This predicted $M(R, t)$ is compared with the data in Fig. 3 inset. Again the prediction is in good agreement with the data.

Several effects modify the simplified theory outlined above. Non-circular drops must have uneven deposition rates: highly convex regions have a stronger evaporating flux and thus denser deposits, as corroborated by Fig. 1a. If the solute is not dilute, the ring deposit is forced to have a non-zero width; higher initial concentration leads to a wider ring. Further thermodynamic effects may modify the flow and the ring deposition. Some solutes may segregate to the substrate surface and become immobilized. Others may segregate to the free surface where the outward flow is faster than $\bar{v}$. The thermal and concentration gradients caused by evaporation can lead to circulating flows driven by surface-tension gradients (that is, Marangoni flows). These can interfere with the outward flow discussed above. Our experiments showed both surface segregation and circulating flow but their effect was minor (as we will discuss in detail elsewhere). High viscosity in the liquid can also modify the deposition by preventing the drop from attaining an equilibrium droplet shape. We estimate that in our experiments such viscous effects should be negligible except within a few micrometres on the contact line.

Our measurements support this capillary flow mechanism for contact-line deposition. They show that the deposition can be predicted and controlled without knowing the chemical nature of the liquid, solute or substrate. The model accounts in a natural way for the nearly complete transport of the solute to the periphery: it also predicts that we can control the shape and thickness of the deposit by controlling the speed and spatial variation of the evaporation. Often it is desired to deposit solute particles in a confined region as, for example, in the printing of fine lines[5]. The commonplace ring stain seems to provide a simple and robust route to such a goal. □

Received 1 May; accepted 26 August 1997.

1. Parisse, F. & Allain, C. Shape changes of colloidal suspension droplets during drying. *J. Phys. II* **6,** 1111–1119 (1996).
2. El Bediwi, A. B., Kulnis, W. J., Luo, Y., Woodland, D. & Unertl, W. N. Distributions of latex particles deposited for water suspensions. *Mater. Res. Soc. Symp. Proc.* **372,** 277–282 (1995).
3. Denkov, N. D. *et al*. Mechanism of formation of two-dimensional crystals from latex particles on substrates. *Langmuir* **8,** 3183–3190 (1992).
4. Laden, P. (ed.) *Chemistry and Technology of Water Based Inks* (Blackie Academic & Professional, London, 1997).
5. *TAPPI New Printing Technologies Symposium 1996* (TAPPI Press, Atlanta, 1996).
6. Hisatake, K., Tanaka, S. & Aizawa, Y. Evaporation of water in a vessel. *J. Appl. Phys.* **73,** 7395–7401 (1993).
7. Peiss, C. N. Evaporation of small water drops maintained at constant volume. *J. Appl. Phys.* **65,** 5235–5237 (1989).
8. Maxwell, J. C. *Scientific Papers* Vol. 2 (Cambridge, 1890).
9. Jackson, J. D. *Classical Electrodynamics* 2nd edn, 77 (Wiley, New York, 1975).
10. Lide, D. R. (ed.) *CRC Handbook of Physics and Chemistry* 77th edn, 6–8, 6–218 (Chemical Rubber Publishing Co., Boca Raton, FL, 1996).
11. Crocker, J. C. & Grier, D. G. Methods of digital video microscopy for colloidal studies. *J. Colloid Interface Sci.* **179,** 298–310 (1996).

Acknowledgements. We thank H. Li, X. Shi and M. Baildon for their early contributions to this project; J. Crocker, D. Grier and A. Marcus for sharing their expertise, their image analysis code and their facilities; and S. Garoff, L. Mahadevan, S. Esipov, R. Leheny, D. Mueth, E. Ehrichs, J. Knight, S. Blanton, N. Menon, J. Cina and L. Kadanoff for discussions. This work was supported by the NSF-MRSEC, NSF and DOE.

Correspondence should be addressed to R.D.D. (e-mail: ddeegan@cotnrol.uchicago.edu). Further information on ring stains may be found at http://MRSEC.uchicago.edu/MRSEC.

Polymerized colloidal crystal hydrogel films as intelligent chemical sensing materials

John H. Holtz & Sanford A. Asher

Department of Chemistry, University of Pittsburgh, Pittsburgh, Pennsylvania 15260, USA

Chemical sensors[1] respond to the presence of a specific analyte in a variety of ways. One of the most convenient is a change in optical properties, and in particular a visually perceptible colour change. Here we report the preparation of a material that changes colour in response to a chemical signal by means of a change in diffraction (rather than absorption) properties. Our material is a crystalline colloidal array[2–12] of polymer spheres (roughly 100 nm diameter) polymerized within a hydrogel[13,14] that swells and shrinks reversibly in the presence of certain analytes (here metal ions and glucose). The crystalline colloidal array diffracts light at (visible) wavelengths determined by the lattice spacing[2–12], which gives rise to an intense colour. The hydrogel contains either a molecular-recognition group that binds the analyte selectively (crown ethers for metal ions), or a molecular-recognition agent that reacts with the analyte selectively. These recognition events cause the gel to swell owing to an increased osmotic pressure, which increases the mean separation between the colloidal spheres and so shifts the Bragg peak of the diffracted light to longer wavelengths. We anticipate that this strategy can be used to prepare 'intelligent' materials responsive to a wide range of analytes, including viruses.

Many polymer hydrogels change volume in response to marked changes in environmental conditions, such as temperature, solvent and pH[15–27]. For certain gel characteristics, these volume changes can be abrupt (volume transitions) as the control parameter is varied. To use such volume changes for chemical sensing, functional groups can be attached to the polymer chains that interact selec-

tively with a single solute species. Such intelligent hydrogels might be used in chemomechanical systems[28–30] and separation devices[31–33] as well as sensors[34–36]. We have recently exploited this kind of response in a temperature-switchable optical diffraction device consisting of a crystalline colloidal array (CCA) polymerized within a hydrogel that responds to temperature changes[13].

Our sensor materials use a three-dimensional periodic CCA of highly charged polystyrene spheres ~100 nm in diameter to report on the gel volume. Because of electrostatic interactions the spheres self-assemble into a body-centred or face-centred cubic (BCC or FCC) array with a mesoscale periodicity (roughly 100–1,000 nm); thus, the CCA Bragg-diffracts visible light[2–5]. The diffraction is in the dynamical diffraction regime, and almost[5] follows Bragg's law:

$$m\lambda = 2nd\sin\theta$$

where m is the diffraction order, λ is the wavelength of light in vacuum, n is the refractive index of the system, d is the diffracting plane spacing, and θ is the Bragg glancing angle.

We fabricate polymerized crystalline colloidal arrays (PCCA) by dissolving non-ionic polymerizable monomers within the CCA suspension and photopolymerizing these species into a hydrogel which entraps the CCA lattice[14]. Thus, the CCA lattice spacing, and hence the diffracted wavelength, depends on the hydrogel volume. A change of 0.5% in the hydrogel volume shifts the diffraction by ~1 nm.

We fabricated an intelligent PCCA (IPCCA) sensitive to Pb^{2+}, Ba^{2+} and K^+ by copolymerizing 4-acryloylaminobenzo-18-crown-6 (AAB18C6) into the PCCA. This crown ether selectively complexes Pb^{2+}, Ba^{2+} and K^+ (refs 37–39). Crown ether binding of these particular cations localizes charges onto the gel network (Fig. 1). The gel swelling mainly results from an increased osmotic pressure within the gel due to a Donnen potential arising from mobile counterions to the crown ether bound cations[21,27,40]. The cation binding forms a polyelectrolyte hydrogel, whose charge state is determined only by the number of cations bound; the degree of swelling of polyelectrolyte gels increases with the number of covalently attached charged groups[21,27,40].

Figure 2 shows that the IPCCA volume and diffraction wavelength monotonically increase with increasing Pb^{2+} concentrations between 0.1 μM (~20 p.p.b.) and 10 mM (~2,000 p.p.m.), at moderate ionic strengths of non-interfering electrolytes (<1 mM LiCl, for example); the shift in the IPCCA diffraction induced by 20 μM $Pb(CH_3COO)_2$ (4 p.p.m.) is easily visible to the naked eye. The hydrogel volume maximum occurs at ~10 mM Pb^{2+} where the crown ethers become saturated. At higher Pb^{2+} concentrations the gel begins to shrink because of the decrease in the Donnan osmotic pressure at higher ionic strengths[21,27,40]. The swelling is reversible; the diffraction reverts to its original wavelength when Pb^{2+} is exchanged out by soaking for a few minutes in de-ionized water. The diffraction peak maxima of the PCCA were reproducible to within 1–2 nm over 200 successive washings and re-immersions in Pb^{2+} solutions.

The selectivity of the IPCCA sensor volume response is determined by the selectivity of the incorporated molecular recognition agent. For example, the 18-crown-6 complex shows log K values (K is the equilibrium binding constant) of 0.8, 2.03, 3.87 and 4.27 for Na^+, K^+, Ba^{2+} and Pb^{2+} respectively[37–39]. Thus, Ba^{2+} swells the PCCA almost identically to Pb^{2+}, making it the major interfering species; K^+ competes with Pb^{2+} for binding only for K^+ concentrations ~200 times that of the Pb^{2+}, and 2,000-fold excess Na^+ is required to compete with Pb^{2+} binding.

Ions that are not complexed by the crown ether only interfere with the IPCCA Pb^{2+} response at relatively high concentrations, because of the impact of their ionic strength on decreasing the

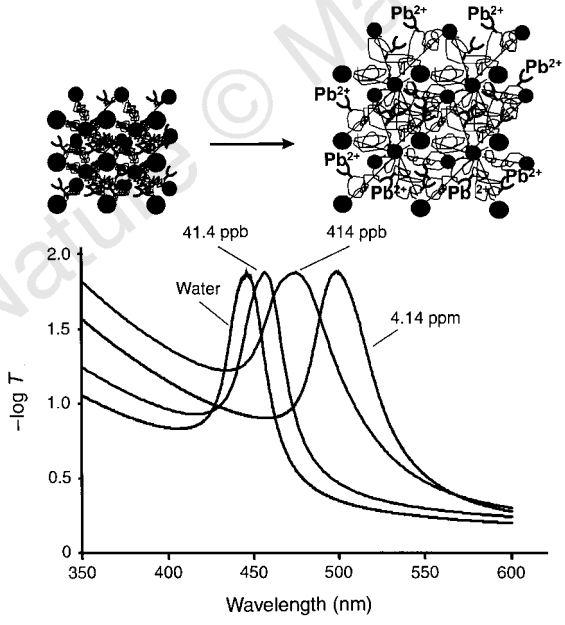

Figure 1 Visible extinction spectra of an acrylamide IPCCA Pb^{2+} sensor at various concentrations of $Pb(CH_3COO)$. The ordinate is given as –log T, where T is the transmittance. The extinction spectra were measured at normal incidence during immersion of the IPCCA in different Pb^{2+} solutions by using a Perkin-Elmer Lambda-9 ultraviolet–visible spectrophotometer. The IPCCA consists of ~7 wt% polystyrene particles, and ~5 wt% total of polymerizable monomer, cross-linker and crown ether. The relative composition of polymerizable monomers was: 86 wt% acrylamide (AMD), 17 wt% AAB18C6 and 7 wt% *N*,*N*′-methylenebisacrylamide (bis AMD), the cross-linker. There is roughly 1 crown ether per 20 AMD, giving an average separation of ~3 nm for a random distribution of crown ether groups.

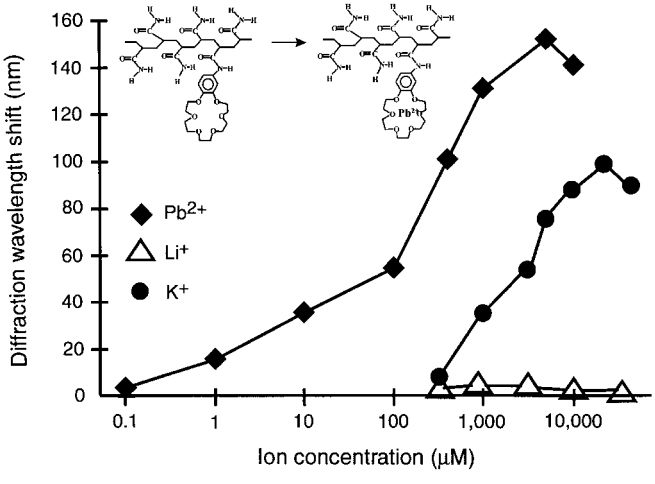

Figure 2 Dependence of the diffracted wavelength of the PCCA sensor on the concentration of cations bound by the crown ether. The cation Pb^{2+} is complexed most strongly, K^+ is more weakly bound, and Li^+ binds negligibly. The diffraction peak maximum redshifts with increasing binding of cations. At very high concentrations of complexed ion, the PCCA contracts slightly, causing a small diffraction blueshift. The detectable concentration range for Pb^{2+} is between 2 μM and 10 mM.

Donnan osmotic pressure. For example 1 mM concentrations of Li^+ and H^+ do not affect the response to 1 μM Pb^{2+}. However, concentrations of ~200 mM dramatically decrease the response to Pb^{2+}. The ions Fe^{3+}, Cu^{2+} and Cd^{2+}, which interfere with electrochemical determinations of Pb^{2+} in water[41–43], have no effect on the response to 1 μM Pb^{2+} at 10 μM concentrations. But at concentrations of 100 μM the volume response to Pb^{2+} decreases, and at 20 mM little response to Pb^{2+} is evident.

We also fabricated an IPCCA glucose sensor by attaching the enzyme glucose oxidase (GOx) to a PCCA of polystyrene colloids. We hydrolysed the PCCA, biotinylated it, and attached[44] ~20 mg of avidinated GOx cubic centimetre of PCCA, giving a spacing of ~25 nm between enzymes. Glucose solutions prepared in air cause the IPCCA to swell and redshift the diffraction as shown in Fig. 3. No response occurs for similar concentrations of sucrose or mannose, because of the enzyme selectivity. The swelling saturates above 0.5 mM glucose because of the formation of a steady state for the conversion of glucose to gluconic acid, coupled to the reoxidation of the GOx by dissolved oxygen. This IPCCA returns to its original diffraction wavelength after removal from glucose.

The IPCCA swelling results from formation of a reduced flavin anion upon glucose turnover. The oxidized flavin is uncharged at neutral pH; however, the reduced flavin is anionic at pH 7 (ref. 45). The reduced flavin is reoxidized by O_2:

$$\text{GOx(ox)} + \text{glucose} \rightarrow \text{GOx}^-\text{(red)} + \text{gluconic acid} + H^+$$

$$H^+ + \text{GOx}^-\text{(red)} + O_2 \rightarrow H_2O_2 + \text{GOx(ox)}$$

The swelling response to glucose decreases at high ionic strength because of the decrease in the Donnan osmotic pressure.

The concentration of anionic, reduced flavins at steady state depends on the concentrations of both glucose and dissolved oxygen. In the absence of oxidants, the gel responds even to glucose concentrations of 10^{-12} M; the diffraction is redshifted 8 nm within 30 min if the solution is stirred. At constant glucose concentrations, the number of anionic, reduced flavins depends upon the dissolved oxygen concentration (Fig. 4). Reoxidation of the flavin shrinks the IPCCA because the number of hydrogel charges is reduced.

We also used the Pb^{2+} IPCCA as an optrode sensor by attaching a small piece of the IPCCA to the end of an optical fibre. We coupled light into the fibre and detected the light back-diffracted into the fibre. This optrode worked as a dip probe to monitor low concentrations of Pb^{2+} remotely.

The 125-μm-thick IPCCAs reach equilibrium in seconds to minutes, depending on analyte concentration. The 125-μm-thick Pb^{2+} IPCCA reaches equilibrium in 1 mM Pb^{2+} within 30 s, and the 125-μm-thick glucose IPCCA reaches equilibrium in 0.1 mM glucose within 2 min. The response rate of the Pb^{2+} IPCCA is limited only by analyte diffusion and the collective diffusion of the hydrogel network[46], whereas enzyme IPCCA responses can also be limited by enzyme kinetics. Decreasing the IPCCA thickness, and the monomer and cross-linker content of the hydrogels, markedly increases the response rate. For example, 10-μm-thick IPCCAs should respond within milliseconds; diffraction from these thin IPCCAs are easily visible to the eye.

The swelling of these IPCCAs results from immobilization of charges on the crown ether or the enzyme-bound flavin. As in all polyelectrolyte gels[21,27,40] swelling results from the competition between the Donnan osmotic pressure and the elasticity of the gel network[21]. This osmotic pressure increases monotonically with the number of bound charges, but begins to decrease at high ionic strengths[21]. However, the glucose IPCCA still responds to 0.1 mM glucose in 0.1 mM NaCl, and the Pb^{2+} IPCCA swells in response to 0.1 mM Pb^{2+} in 50 mM NaCl solutions. We will discuss these

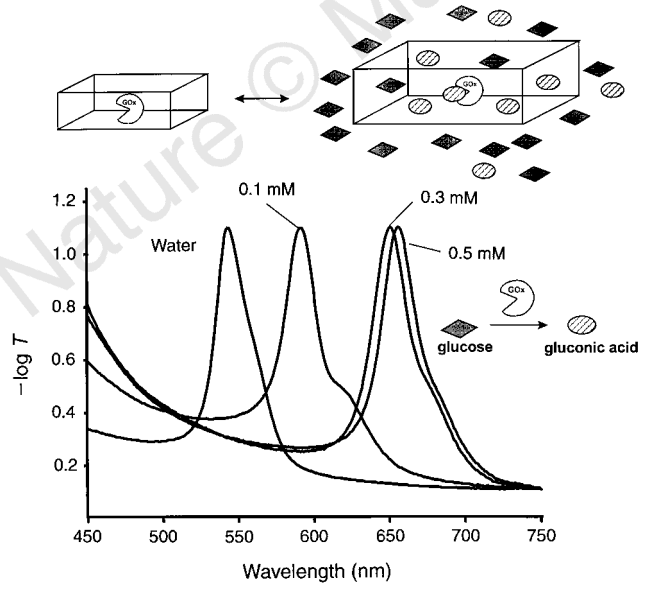

Figure 3 Visible extinction spectra showing how diffraction depends on the glucose concentration for the 125-μm-thick PCCA glucose sensor. The ordinate is given as –log *T*, where *T* is the transmittance. The IPCCA expands for concentrations between 0.1 and 0.5 mM glucose. This IPCCA was polymerized from a solution containing ~7 wt% polystyrene colloidal spheres, 4.6 wt% AMD and 0.4 wt% bisAMD, with water constituting the remaining fraction. This hydrogel was hydrolysed in a solution of NaOH and was then biotinylated with biotinamidopentylamine, which was attached using a water-soluble carbodiimide coupling agent. Avidinated glucose oxidase was then directly added to the PCCA.

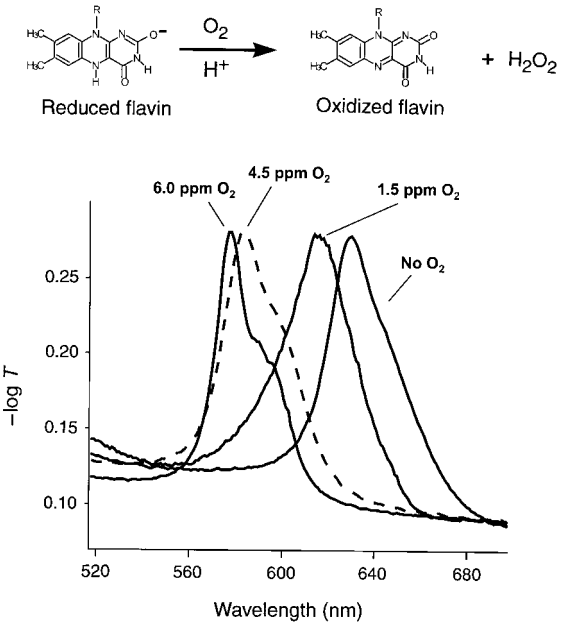

Figure 4 Extinction spectra of the PCCA glucose sensor immersed in an aqueous solution of 0.2 mM glucose with varying O_2 concentrations. The ordinate is given as –log *T*, where *T* is the transmittance. The sensor diffracted at 545 nm in the absence of glucose.

phenomena in more detail elsewhere (J. H. H., J. S. W. Holtz, C. H. Munro and S. A. A., manuscript in preparation). Obviously we can tailor the dynamic range of these IPCCAs by controlling the number and affinity of the molecular recognition agents and by altering the elasticity[21,46–49] of the gel network to define the dynamic range of the sensor response. These sensors could also be used at very high ionic strengths by sample preparation procedures such as dilution or ion exchange.

We can directly quantify the IPCCA response to samples of different ionic strengths by determining the ionic strength using a second polyelectrolyte PCCA gel; we have similarly fabricated a hydrolysed acrylamide PCCA that shrinks in response to ionic strength.

We are also developing IPCCA that do not use bound charges. For example, we can use recognition agents that alter the volume phase transition temperature[13] as analytes bind to the recognition elements. In addition, we can use recognition agents that alter the free energy of mixing upon analyte binding to alter the IPCCA volume[21].

Using the same general motif for creating sensor materials and devices but incorporating other crown ethers could produce IPCCAs sensitive to cations other than Pb^{2+}, Ba^{2+} and K^{+}. With the use of the avidin–biotin interaction, numerous biomolecular recognition elements could be incorporated into the PCCA. For example, we expect to be able to bind recognition elements such as HIV antibodies in order to fabricate sensors that respond to low virus concentrations.

We expect to use IPCCAs in arrays of optical sensors, where each individual sensor will detect different analytes and different concentration ranges. The diffraction from these IPCCAs is easily visible and can be used for simple colour tests for analytes in solution; the perceived blue diffraction from a 2 μM Pb^{2+} solution shifts to green for a 20 μM Pb^{2+} solution. This technology may prove useful in simple kits for environmental or clinical diagnostics. □

Received 14 May; accepted 18 August 1997.

1. Janata, J. *Principles of Chemical Sensors* (Plenum, New York, 1989).
2. Carlson, R. J. & Asher, S. A. Characterization of optical diffraction and crystal structure in monodisperse polystyrene colloids. *Appl. Spectrosc.* **38,** 297–304 (1984).
3. Asher, S. A. Crystalline narrow band radiation filter. U.S. Patent Nos 4,627,689 and 4,632,517.
4. Asher, S. A., Flaugh, P. L. & Washinger, G. Crystalline colloidal Bragg diffraction devices: The basis for a new generation of Raman instrumentaiton. *Spectroscopy* **1,** 26–31 (1986).
5. Rundquist, P. A., Photinos, P., Jagannathan, S. & Asher, S. A. Dynamical Bragg diffraction from crystalline colloidal arrays. *J. Chem. Phys.* **91,** 4932–4941 (1989).
6. Krieger, I. M. & O'Neill, F. M. Diffraction of light by arrays of colloidal spheres. *J. Am. Chem. Soc.* **90,** 3114–3120 (1968).
7. Hiltner, P. A. & Krieger, I. M. Diffraction of light by ordered suspensions. *J. Phys. Chem.* **73,** 2386–2389 (1969).
8. Hiltner, P. A., Papir, Y. S., Krieger, I. M. Diffraciton of light by nonaqueous ordered suspensions. *J. Phys. Chem.* **75,** 1881–1886 (1971).
9. Clark, N. A., Hurd, A. J. & Ackerson, B. J. Single colloidal crystals. *Nature* **281,** 57–60 (1979).
10. Ackerson, B. J. & Clark, N. A. Shear-induced melting. *Phys. Rev. Lett.* **46,** 123–126 (1981).
11. Aastuen, D. J. W., Clark, N. A., Cotter, L. K. & Ackerson, B. J. Nucleation and growth of colloidal crystals. *Phys. Rev. Lett.* **57,** 1733–1736 (1986).
12. Hurd, A. J., Clark, N. A., Mockler, R. C. & O'Sullivan, W. Lattice dynamics of colloidal crystals. *Phys. Rev.* A**26,** 2869–2881 (1982).
13. Weissman, J. M., Sunkara, H. B., Tse, A. S. & Asher, S. A. Thermally switchable periodicities and diffraction from novel mesocopically ordered materials. *Science* **274,** 959–960 (1996).
14. Asher, S. A., Holtz, J., Liu, L. & Wu, Z. Self assembly motif for creating submicron periodic materials. Polymerized crystalline colloidal arrays. *J. Am. Chem. Soc.* **116,** 4997–4998 (1994).
15. Dusek, K. (ed.) *Responsive Gels: Volume Phase Transitions, Advances in Polymer Science* **109,** (Springer, Berlin, 1993).
16. Dusek, K. (ed.) *Responsive Gels: Volume Phase Transitions II, Advances in Polymer Science* 110 (Springer, Berlin, 1993).
17. Okano, T. Molecular design of temperature-responsive polymers as intelligent materials. *Adv. Polym. Sci.* **110,** 179–197 (1993).
18. Kataoka, K., Miyazaki, H., Okano, T. & Sakurai, Y. Sensitive glucose-induced change of the lower critical solution temperature. *Macromolecules* **27,** 1061–1062 (1994).
19. Irie, M. Stimuli-responsive poly(N-isopropylacrylamide). Photo- and chemical-induced phase transitions. *Adv. Polym. Sci.* **110,** 49–65 (1993).
20. Irie, M., Misumi, Y. & Tanaka, T. Stimuli-responsive polymers: Chemical induced reversible phase separation of an aqueous solution of poly(N-isopropylacrylamide) with pendent crown ether groups. *Polymer* **34,** 4531–4535 (1993).
21. Flory, J. *Principles of Polymer Science* (Cornell Univ. Press, Ithaca, 1953).
22. Kubota, K., Fujishige, S. & Ando, I. Single-chain transition of poly(N-isopropylacrylamide) in water. *J. Phys. Chem.* **94,** 5154–5158 (1990).
23. Fujishige, S., Kubota, K. & Ando, I. Phase transition of aqueous solutions of poly(N-isopropylacrylamide) and poly(N-isopropylmethacrylamide). *J. Phys. Chem.* **93,** 3311–3313 (1989).
24. Schild, H. G. Poly(N-isopropylacrylamide): Experiment, theory and application. *Prog. Polym. Sci.* **17,** 163–249 (1992).
25. Heskins, M. & Guillet, J. E. Solution properties of poly(N-isopropylacrylamide). *J. Macromol. Sci. Chem.* A**2,** 1441–1455 (1968).
26. Tanaka, T. Collapse of gels and the critical endpoint. *Phys. Rev. Lett.* **40,** 820–823 (1978).
27. Khokhlov, A. R. & Kramarenko, E. Yu. Weakly charged polyelectorlytes: collapse induced by extra ionization. *Macromolecules* **29,** 681–685 (1996).
28. Gehrke, S. H. Synthesis, equilibrium swelling, kinetics, permeability and applications of environmentally responsive gels. *Adv. Polym. Sci.* **110,** 81–144 (1993).
29. Osada, Y. & Gong, J. Stimuli responsive gels and their application ot chemomechanical systems. *Prog. Polym. Sci.* **18,** 187–226 (1993).
30. Kataoka, K., Kyoy, H. & Tsuruta, T. Novel pH-sensitive hydrogels of segmented poly(amine ureas) having a repetitive array of polar and apolar units in the main chain. *Macromolecules* **28,** 3336–3341 (1995).
31. Wang, K. L., Burban, J. H. & Cussler, E. L. Hydrogels as separation agents. *Adv. Polym. Sci.* **110,** 67–79 (1993).
32. Gehrke, S. H., Andrews, G. P. & Cussler, E. L. Chemical aspects of gel extraction. *Chem. Eng. Sci.* **41,** 2153–2160 (1986).
33. Grimshaw, P. E., Grodzinski, A. J., Yarmush, M. L. & Yarmush, D. M. Dynamical membranes for protein transport: Chemical and electrical control. *Chem. Eng. Sci.* **44,** 827–840 (1989).
34. Sheppard, N. F., Lesho, M. J., McNally, P. & Francomacaro, A. S. Microfabricated conductometric pH sensor. *Sensors and Actuators B* **28,** 95–102 (1995).
35. Schalkhammer, T. *et al.* The use of metal-island-coated pH-sensitive swelling polymers for biosensor applications. *Sensors and Actuators B* **24/25,** 166–172 (1995).
36. McCurley, M. F. An optical biosensor using a fluorescent, swelling sensing element. *Biosensors Biolectr.* **9,** 527–533 (1994).
37. Lamb, J. D., Izatt, R. M., Christiansen, J. J. & Eatough, D. J. Thermodynamics and kinetics of cation-macrocycle interaction in *Coordination Chemistry of Macrocylic Compounds* (ed. Melson, G. A.) (Plenum, New York, 1979).
38. Izatt, R. M. *et al.* Calorimetric titration study of the interaction of some uni- and bivalent cations with benzo-15-crown-5, 18-crown-6, dibenzo-24-crown-8 and dibenzo-27-crown-9 in methanol–water solvents, at 25 °C and μ = 0.1. *J. Am. Chem. Soc.* **98,** 7626–7630 (1976).
39. Kopolow, S., Hogan Esch, T. E. & Smid, J. Poly(vinyl macrocyclic polyethers). Synthesis and cation binding properties. *Macromolecules* **6,** 133–142 (1973).
40. Hirotsu, S., Hirokawa, Y. & Tanaka, T. Volume-phase transitions of ionized N-isopropylacrylamide gels. *J. Chem. Phys.* **87,** 1392–1395 (1987).
41. Zen, J. M. & Huang, S. Y. Square-wave voltammetric determination of lead(II) with a Nafion/2,2 bipyridyl mercury film electrod. *Anal. Chim. Acta* **296,** 77–86 (1994).
42. Yokoi, K., Yamaguchi, A., Mizumachi, M. & Koide, T. Direct determination of trace concentrations of lead in fresh water samples by adsorptive cathodic stripping voltammetry of a lead-calcein blue complex. *Anal. Chim. Acta* **316,** 363–369 (1995).
43. Dubey, R. K. & Puri, B. K. Simultaneous determination of lead and cadmium in various environmental and biological samples by differential pulse polarography after adsorption of their morpholine-4-carbodithioates onto microcrystalline naphthalene or morpholine-4-dithiocarbamate-CTMAB-napthalene adsorbent. *Talanta* **42,** 65–72 (1995).
44. Savage, M. D. *et al. Avidin–Biotin Chemistry: A Handbook* (Pierce Chemical Company, Rockford IL, 1992).
45. Raba, J. & Mottola, H. Glucose oxidase as an analytical reagent. *Crit. Rev. Anal. Chem.* **25,** 1–42 (1995).
46. Li, Y. & Tanaka, T. Kinetics of swelling and shrinking of gels. *J. Chem. Phys.* **92,** 1365–1371 (1990).
47. Fillmore, D. J. & Tanaka, T. Kinetics of swelling of gels. *J. Chem. Phys.* **70,** 1214–1218 (1979).
48. Peters, A. & Candau, S. J. Kinetics of swelling of polyacrylamide gels. *Macromolecules* **19,** 1952–1955 (1986).
49. Hakiki, A. & Herz, J. E. A study of the kinetics of swelling in cylindrical polystyrene gels: Mechanical behavior and final properties after swelling. *J. Chem. Phys.* **101,** 9054–9059 (1994).

Acknowledgements. We thank C. Munro for assistance with the optical fibre measurements, and S. G. Weber and R. C. Coalson for discussions. This work was supported by the Office of Naval Research, the Air Force Office of Scientific Research and the National Science Foundation.

Correspondence should be addressed to S.A.A. (e-mail: asher+@pitt.edu).

Solvent-assisted proton transfer in catalysis by zeolite solid acids

James F. Haw*, Teng Xu*, John B. Nicholas† & Patrick W. Goguen*

* *The Laboratory for Magnetic Resonance and Molecular Science, Department of Chemistry, Texas A&M University, College Station, Texas 77843, USA*

† *Environmental Molecular Science Laboratory, Pacific Northwest National Laboratory, Richland, Washington 99352, USA*

Intermolecular proton transfer in the gas phase is usually strongly disfavoured because the charged products are highly unstable. It is promoted in aqueous solution, however, because the high dielectric constant ($\epsilon = 78.3$) of water allows efficient stabilization of the corresponding cations and anions. Zeolites—microporous catalysts used in petroleum refining and the synthesis of chemical feedstocks—provide another medium for proton-transfer reactions[1–3], because their anionic aluminosilicate frameworks are highly acidic. The low dielectric constant of zeolites ($\epsilon \approx 1.6$; ref. 3) suggests, however, that such processes in the zeolite